

01 Apr 2022

Modelling and Validation of a Gas-Solid Fluidized Bed using Advanced Measurement Techniques


Sebastián Uribe

Haidar Taofeeq

Muthanna H. Al-Dahhan

Missouri University of Science and Technology, aldahhanm@mst.edu

Follow this and additional works at: https://scholarsmine.mst.edu/che_bioeng_facwork

 Part of the [Biomedical Engineering and Bioengineering Commons](#), and the [Chemical Engineering Commons](#)

Recommended Citation

S. Uribe et al., "Modelling and Validation of a Gas-Solid Fluidized Bed using Advanced Measurement Techniques," *Canadian Journal of Chemical Engineering*, vol. 100, no. S1, pp. S272 - S287, Wiley, Apr 2022. The definitive version is available at <https://doi.org/10.1002/cjce.24070>

This Article - Journal is brought to you for free and open access by Scholars' Mine. It has been accepted for inclusion in Chemical and Biochemical Engineering Faculty Research & Creative Works by an authorized administrator of Scholars' Mine. This work is protected by U. S. Copyright Law. Unauthorized use including reproduction for redistribution requires the permission of the copyright holder. For more information, please contact scholarsmine@mst.edu.

ARTICLE

Modelling and validation of a gas-solid fluidized bed using advanced measurement techniques

 Sebastián Uribe¹  | Haidar Taofeeq^{2,3} | Muthanna Al-Dahhan^{1,4}

¹Chemical and Biochemical Engineering Department, Missouri University of Science and Technology, Rolla, Missouri, USA

²Chemical Engineering Department, College of Engineering, Al-Nahrain University, Baghdad, Iraq

³Prosthetics and Orthotics Engineering Department, College of Engineering, Al-Nahrain University, Baghdad, Iraq

⁴Mining and Nuclear Engineering Department, Missouri University of Science and Technology, Rolla, Missouri, USA

Correspondence

Muthanna Al-Dahhan, Chemical and Biochemical Engineering Department, Missouri University of Science and Technology, Rolla, MO 65409 USA; Mining and Nuclear Engineering Department, Missouri University of Science and Technology, Rolla, Missouri 65409, USA.

Email: aldahhanm@mst.edu

Abstract

With a Euler-two-phase (E2P) approach, through computational fluid dynamics (CFD) techniques, a mathematical model for the prediction of the local hydrodynamic behaviour of a gas-solid fluidized bed was implemented. Simulations are conducted for a fluidized bed of 0.14 m internal diameter packed with Gerdart B glass beads particles, with an average diameter of 365 μm , at dimensionless inlet velocities ranging from $\frac{\langle V_{\beta} \rangle_0}{V_{mf}} = 1.6 - 2.14$. The implemented model considers the multiphase and multiscale interactions through the inclusion of three sub-models, which allows the model to have a broad range of applicability. Predictions were compared against experimental measurements reported on previous contributions for validation purposes. The experimental study was conducted by implementing advanced measurement techniques, such as a differential pressure transducer, and an optical fibre probe for simultaneous measurement of solids holdup and velocity, developed at the Multiphase Flow and Reactors Engineering and Applications Laboratory (mFReal). Local radial solids holdup, solids velocity, and pressure drop profiles were experimentally determined. Results show that the implemented model possesses a high predictive quality, predicting pressure drops with an average absolute relative error (AARE) between 8.6%–11.3%; solids holdup with a root mean squared deviation (RMSD) under 5%; and solids velocity with a RMSD under 22%.

KEYWORDS

CFD modelling, Euler-two-phase model, fluidized bed, optical fibre sensor

1 | INTRODUCTION

Despite the vast industrial applications of gas-solid fluidized beds, such as fluid catalytic cracking, combustion and gasification, drying, and other processes,^[1–6] the flow structures and mixing behaviours inside these systems are poorly understood.^[7,8] An accurate understanding and prediction of these hydrodynamic parameters on fluidized beds is of paramount importance in order to develop scale-up methodologies and to enhance the reactors' throughput. One of the main reasons of this lack of

a deeper understanding lies in the complexity of the multiphase interactions and the inherent multiscale nature of fluidized beds.

In this sense, with different approaches, for different length scales, and with different setups and techniques, many experimental efforts in the evaluation of the key hydrodynamic parameters on fluidized beds, such as solids holdup, bubble rise velocity, bubble size and frequency, and solids particle velocity, can be found in the literature.^[1,5,9–12] However, the level of detail and accuracy in the description of the local scale phenomena in

these studies is limited by the applied measurement techniques, leading to systematic differences in the predictions.^[12] Furthermore, most of the experimental techniques do not allow to access the pointwise changes in the fields (velocity, holdup, pressure) at local time scales, and are usually limited to a restricted number of locations inside the bed.^[6,13]

An important contribution to the experimental studies of fluidized beds are the works of Taofeeq et al.,^[1,8,13–15] who extensively explored the use of optical fibre probes and differential pressure transducer to determine local radial profiles of solids holdup, solids velocity, bubble rise velocity, bubble frequency, bubble chord length, and local pressure drops. In their contributions, the effect of different configurations of immersed vertical internals and different Geldart B solid particles materials (glass beads and aluminium oxide, with average diameters of $D_\sigma \approx 360 \mu\text{m}$) over these hydrodynamic parameters was studied under different air flow rates. The use of different configurations on the experimental setup and application of advanced measurement techniques allowed for the development of a comprehensive study of the phenomena present inside the column under different scenarios, and it was possible to obtain the time series variation of the measured parameters. However, it is important to note that the measurements with the 2-tip optical probes and the differential pressure transducer were taken at five different radial locations at three different heights, thus overlooking the differences in the radial profiles at different angular positions.

An alternative and promising tool to study the local hydrodynamic behaviour of fluidized bed can be found in the application of computational fluid dynamics (CFD) techniques. The application of these mathematical modelling tools allows access to the pointwise fields inside the bed and their changes at local times. In the context of modelling fluidized beds, two main approaches have been extensively explored on literature: (a) Eulerian-Eulerian, also referred as Euler-2-phase (E2P) or two-fluid model (TFM),^[4,10,16–19] and (b) Eulerian-Lagrange models, also known as CFD-discrete element model (CFD-DEM), or discrete particle models (DPM).^[20–24] The main difference between these approaches is the treatment of the solid phase. On the CFD-DEM models, the resolved solid particles (Lagrangian phase) are modelled; solving equations of motion for each individual particle, the fluid phase is accounted as a continuum (Eulerian phase), and the interactions between these two phases is accounted through interfacial exchange closure models. Modelling real scale systems, with up to millions of solid particles, or modelling systems with very small solid particle sizes ($O(D_\sigma) \leq 500 \mu\text{m}$) through CFD-DEM becomes impractical, and usually is limited by the

available computational resources. On the other hand, in the E2P models both phases are treated as interpenetrating continuum (i.e., no solid-fluid interphase defined), and the interaction must be included through volumetric exchange closure models. This allows for the modelling of larger scale systems with small solid particle sizes, but usually requires a higher number of coupled sub-models as closures for the multiphysics and multi-scale phenomena.

As suggested above, when modelling the fluidized bed by either of the CFD approaches, a proper selection of the coupled sub-models is required, which should be based on the underlying assumptions for their derivation and their range of applicability. This implies an added level of uncertainty in the mathematical modelling of these systems that cannot be a priori assessed. Therefore, it can be noted that though mathematical modelling of fluidized beds can overcome the limitations discussed for the experimental techniques, there is a fundamental need to validate the models' predictions and assess their predictive quality, which can be achieved by linking models with reliable experiments. In this sense, it should also be pointed out that scale-up and optimization extrapolation studies as well as the study of local behaviours inside the column can only be performed with models with validated predictive quality.

Several studies dealing with the modelling and validation of large-scale fluidized beds with different configurations can be found in the literature. One recent contribution that can be highlighted is the work of Wang et al.^[17] In their work, they coupled an E2P model that accounted for the turbulence through a $k-\varepsilon$ Reynolds-averaged Navier-Stokes (RANS) model with a population balance model (PBM). The PBM was included in order to improve the bubble-emulsion drag force on the E2P model by providing a bubble size distribution. The model included a total of 28 sub-models, incorporating a population balance, bubble coalescence, and bubble breakup sub-models for the bubble dynamics, as well as three momentum exchange closures and a sub-model based on the kinetic theory of granular flow (KTGF) for the multiphase interactions. The KTGF model included a set of empirical and semi-empirical correlations and closures as sub-models to account for the granular viscosity, granular bulk viscosity, frictional viscosity, frictional pressure, granular temperature, solid pressure, and radial distribution. The model consisted of a 2D domain according to the characteristics of the experimental setup used for validation. A good agreement was found between the predicted bubble size distribution and the experimental data of Busciglio et al.^[25] Similarly, Hu and Liu^[26] coupled a PBM model to an E2P model in order to improve its predictive quality. In their model, the PBM

was used to predict the size distribution of solid particles clusters, rather than the bubble size distribution as in the PBM model implemented by Wang et al.^[17] The information of the PBM was used to modify the drag force on the E2P model using an Energy Minimum Multi-Scale (EMMS) theory-based sub-model, and the PBM used the cluster growth rate predicted by a cluster growth sub-model that used the local flow and solids distributions predicted by the E2P model. Their model included a total of 13 sub-models as closures for the KTGF sub-model, the EMMS drag sub-model, and the PBM, which included closures for the solids pressure, granular temperature, solid shear viscosity, diffusion coefficient for granular temperature, solids bulk viscosity, solid radial distribution, collisional dissipation of energy, and coalescence and breakage of the clusters. They compared the model predictions against experimental measurements of axial pressure profiles, and radial gas holdup and solids velocity, reported by Zhou et al.,^[27,28] and important deviations were observed in the local trends. It should be considered that the implemented computational domain was also a 2D domain, which might be a source of their reported deviations in the prediction of the radial gas holdup.

From these two previous modelling examples, it can be seen that the current modelling of fluidized beds strongly relies on the inclusion of a vast number of sub-models, which are usually a set of empirical and semi-empirical expressions. Therefore, the predictive quality of these models is constrained by the applicability of these sub-models, and further uncertainties arise if these models are desired to be used for extrapolation studies. In addition, both models discussed above were validated through the comparison of a single macroscopic parameter (the bubble size distribution), which implies that the quality of the predictions of other local fields, such as holdup and velocity profiles, was not validated.

Thus, it can be seen that despite the advances in the mathematical modelling of fluidized beds through CFD techniques, presently there is no model that has a validated predictive quality and that does not rely on the inclusion of a vast number of sub-models. Therefore, there is no model that can be used to analyze the local behaviours inside the fluidized bed, which are still challenging to measure through experimental techniques. In an effort to overcome these major limitations in the implemented models for fluidized beds, in this work, a simplified model which captures the essential multiphase and multiscale interactions is developed, implemented, and locally validated. The simplified model is based on an E2P formulation and includes a reduced number of sub-models to reduce the uncertainty of its applicability for extrapolation studies. In order to locally validate the

predictive quality of the implemented model, the mathematical modelling study was paired with an experimental study. The experimental measurements were conducted using our in-house developed fast response 2-tip optical fibre probes, developed at the Multiphase Flow and Reactors Engineering and Applications Laboratory (mFReal) from the Missouri University of Science and Technology, as well as a differential pressure transducer probe. These techniques allowed us to obtain local radial profiles of solids holdup, solids velocity, and pressure drops on a fluidized bed without internals, packed with Geldart B type glass beads of average diameter $\langle D_\sigma \rangle = 365 \mu\text{m}$, as reported in previous contributions.^[13,14] The reduction in the number of coupled sub-models to capture the essential multiphase and multiscale interactions, as well as the validation of the predictions against experimentally determined local profiles, represent a significant advance and a promising alternative in the development of a highly predictive model suitable for further extrapolation studies.

2 | CFD MODELLING

2.1 | Geometry

The model's geometrical properties were set to match those of the experimental setup reported by Taofeeq and Al-Dahhan in previous contributions.^[13,14] The geometry of the model consisted of a column with a length of $L_C = 184 \text{ cm}$, where a section with a height of $L_o^0 = 35 \text{ cm}$ was established as the static bed height at initial conditions. Further details of the experimental setup characteristics can be seen in Figure 1, are summarized in Table 1, and will be discussed in the next section,

As seen in Figure 1, the experimental setup consisted of two main sections: the fluidized column and a plenum section for the air inlet and homogenization of the air inflow to the column. In the implemented model, only the fluidized column section is considered, and the plenum section is accounted for through a suitable boundary condition at the inlet of the column.

2.2 | Mesh independency analysis

The geometry and meshing, as well as mathematical models, were implemented in COMSOL Multiphysics 5.4. Mesh independent results were achieved by implementing a mesh of 2.9×10^5 elements. Details of the geometry with internals and the implemented mesh can be seen in Figure 2.

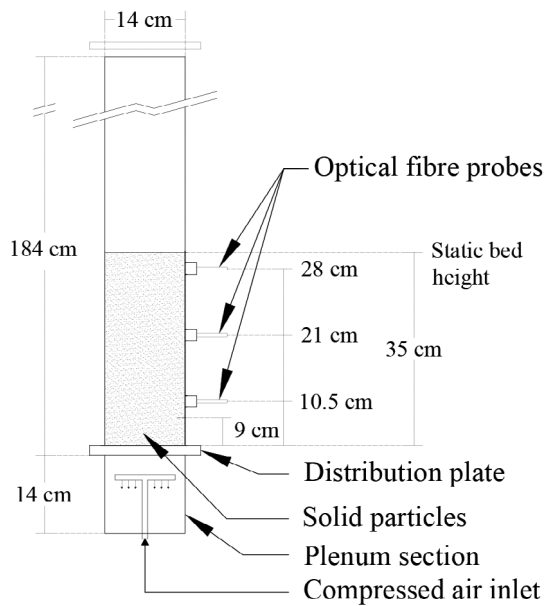


FIGURE 1 Details of the experimental setup

TABLE 1 Geometrical properties of the experimental setup and operation conditions

Geometry	
D_C (cm)	14
L_C (cm)	184
Solids (σ – phase)	
Material	Glass beads
L_σ^0 (cm)	35
$\langle D_\sigma \rangle$ (μm)	365
ρ_σ ($\frac{\text{kg}}{\text{m}^3}$)	2500
Operation conditions	
$\frac{\langle V_\beta \rangle_0}{V_{mf}}$	1.6, 1.76, 1.96, 2.14
V_{mf} ($\frac{\text{m}}{\text{s}}$)	0.4
P_0 (atm)	1

Figure 3 shows a sample of the results of the mesh sensitivity analysis conducted for verifying the independence in the prediction of macroscopic parameters. In the figure, timewise results of overall pressure drops and overall solids holdup for three different meshes are shown. The embedded table shows the relative difference between the prediction of an implemented mesh with respect to the previous smaller one. It can be seen that the relative difference in both metrics when implementing the mesh containing 2.9×10^5 elements is under 5%, suggesting mesh independent results.

The conducted mesh independence analysis also considered the independence of the local predictions.

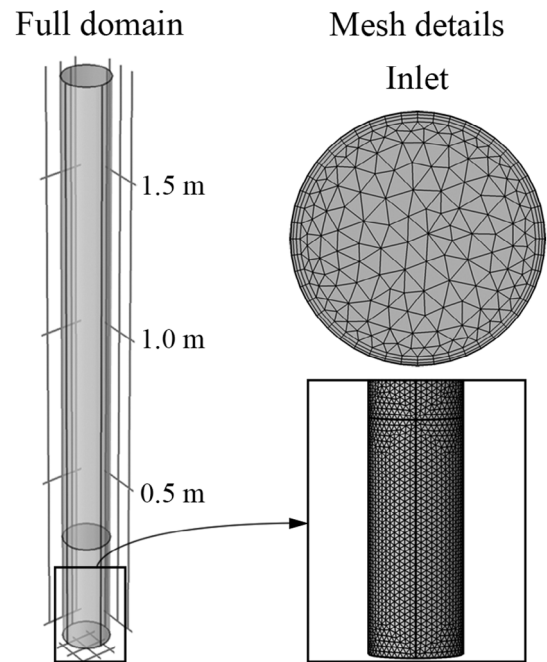


FIGURE 2 Details of the geometry and mesh of the implemented model

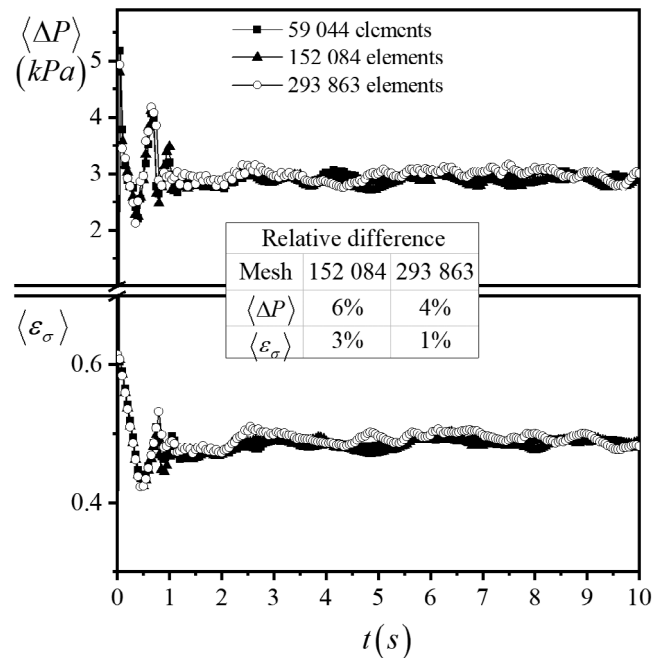


FIGURE 3 Sample of the mesh independency analysis results for the prediction of macroscopic parameters, for a fluidized bed operating at an inlet dimensionless velocity $\langle V_\beta \rangle_0 / V_{mf} = 1.6$

Figure 4 shows a sample of the predicted time-averaged local solids holdup distribution in a fluidized bed operating an inlet dimensionless velocity $\frac{\langle V_\beta \rangle_0}{V_{mf}} = 1.6$, in a cut plane at $\frac{z}{D_C} = 2.0$, for the three different meshes tested. From the qualitative comparison shown in Figure 4, local

differences in the predictions are observed. In order to quantify such differences, and to establish mesh independency in the local predictions, Kolmogorov-Smirnov (KS) tests were conducted to compare the difference in the predicted distributions at different cut planes. As a sample of the local mesh independence analysis, Figure 5A,B shows the statistical comparison of the results shown in Figure 4. Figure 5A shows the histograms of the local solids holdup distributions shown in the cut planes in Figure 4. For better comparison and in order to establish mesh independency, Figure 5B shows the cumulative distribution of these histograms, along with the obtained KS values when comparing an implemented mesh with respect to the previous smaller one. Considering the KS critical value of 0.044, and as

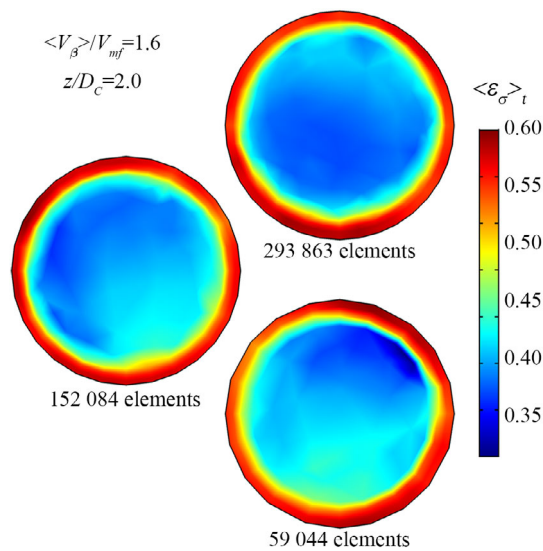


FIGURE 4 Sample of the local mesh independency analysis results, for a fluidized bed operating at inlet dimensionless velocity $\langle V_\beta \rangle / V_{mf} = 1.6$

qualitatively seen in Figure 5B it can be noted that there is a significant difference between the mesh with 59 044 elements and the mesh with 152 084 elements, and that there are no major differences between the finest mesh and the mesh with 152 084 elements. These results suggest that the implemented mesh also allows the mesh independent prediction of local distributions.

2.3 | Governing equations

Given that the solid particles used on the experimental test have small average diameters ($\langle D_\sigma \rangle = 365 \mu\text{m}$), implementing a CFD-DEM model for the fluidized bed would not be practical in terms of the required computational resources and time. By virtue of this, a time dependent E2P approach was selected to model the fluidized bed, where the air was treated as a continuous phase (β - phase) with a dispersed solids continuous pseudo-phase (σ - phase). This implies that both phases, air (β) and solids (σ), are treated as interpenetrating continuum phases and their interactions have to be accounted for through sub-models.

The continuity equations for air and solids (β and σ) are described by Equations (1) and (2), respectively, while Equations (3) and (4) are the momentum balances for air and solids phases (β and σ), respectively. Equation (4) is based on the derivations of Enwald et al.,^[29] which requires the disperse phase (σ - phase) density to be several orders of magnitude larger than the continuous phase (β - phase) density ($\rho_\sigma \gg \rho_\beta$):

$$\frac{\partial(\rho_\beta \varepsilon_\beta)}{\partial t} + \nabla \cdot (\rho_\beta \varepsilon_\beta \mathbf{v}_\beta) = 0 \quad (1)$$

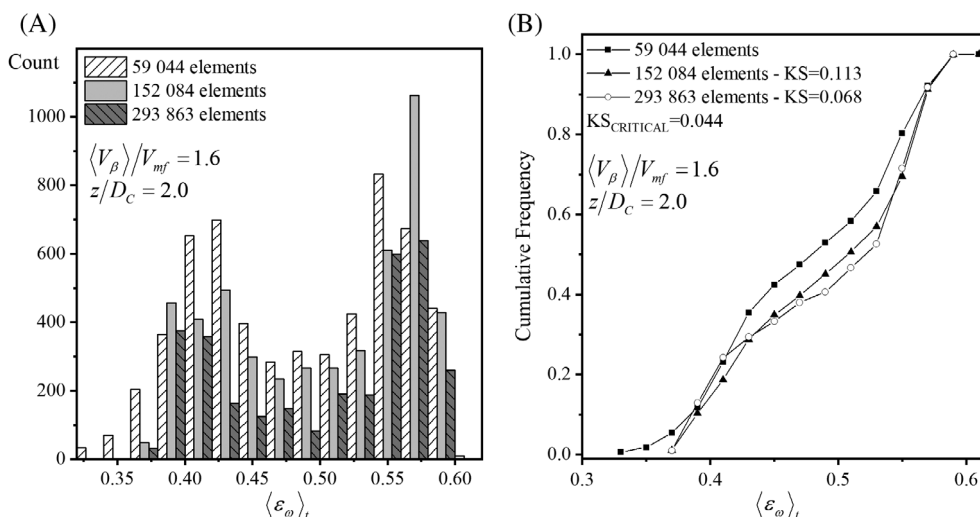


FIGURE 5 (A) Histograms of the solids holdup distributions shown in the cut planes of Figure 4 and (B) Kolmogorov-Smirnov test results

$$\frac{\partial \varepsilon_\sigma}{\partial t} + \nabla \cdot (\varepsilon_\sigma \mathbf{v}_\sigma) = 0 \quad (2)$$

formulation of Ettehadieh et al.,^[30] which is described by Equation (5), and was derived from the experimental

$$\varepsilon_\beta \rho_\beta \left[\frac{\partial \mathbf{v}_\beta}{\partial t} + \mathbf{v}_\beta \nabla \cdot \mathbf{v}_\beta \right] = \varepsilon_\beta \left[-\nabla P + \nabla \cdot \left[\mu_\beta \left(\nabla \mathbf{v}_\beta + (\nabla \mathbf{v}_\beta)^T - \frac{2}{3} (\nabla \cdot \mathbf{v}_\beta) \mathbf{I} \right) \right] + \rho_\beta \mathbf{g} \right] + \mathbf{F}_d \quad (3)$$

$$\varepsilon_\sigma \rho_\sigma \left[\frac{\partial \mathbf{v}_\sigma}{\partial t} + \mathbf{v}_\sigma \nabla \cdot \mathbf{v}_\sigma \right] = -\varepsilon_\sigma \nabla P - G(\varepsilon_\beta) \nabla \varepsilon_\beta + \varepsilon_\sigma \nabla \cdot \left[\mu_{eff} \left(\nabla \mathbf{v}_\sigma + (\nabla \mathbf{v}_\sigma)^T \right) \right] + \varepsilon_\sigma \rho_\sigma \mathbf{g} - \mathbf{F}_d \quad (4)$$

where ρ_i and ε_i are the density and volume fraction of each i -phase, respectively; μ_β is the air viscosity; and μ_{eff} is the effective viscosity of the solid pseudo-phase (i.e., mixture viscosity).

The model described by Equations (1)–(4) requires the inclusion of three sub-models: one to account for the modulus of elasticity ($G(\varepsilon_\sigma)$) on the solids pressure term ($\nabla P_\sigma = G(\varepsilon_\beta) \nabla \varepsilon_\beta$), one to account for the drag force (\mathbf{F}_d), and one to estimate the effective viscosity of the solid pseudo-phase. With these three sub-models, the multiphase interactions and the multiscale phenomena are incorporated in the model.

Equations (3) and (4) have important differences compared with other models that have been implemented for fluidized beds, such as the previously discussed models of Wang et al.^[17] and Verma et al.,^[19] and also with other E2P models that have been implemented in the modelling of similar gas-solid fluidized systems, such as the models implemented by Lan et al.^[16] for a spouted bed. The first difference that can be noted is that on the stress tensor (viscous term) of Equation (3); the viscosity corresponds to that of the pure phase (pure air viscosity), not a mixture viscosity. The second important difference that can be highlighted is that the solids stress-strain tensor is estimated by the contributions of the bed elasticity plus an effective molecular/viscous interaction ($\varepsilon_\sigma \nabla \cdot [\mu_{eff}(\nabla \mathbf{v}_\sigma + (\nabla \mathbf{v}_\sigma)^T)]$). Therefore, there is no inclusion of a sub-model such as the KTGF model that further requires of a set of correlations, closures, and other sub-models to estimate effective parameters such as granular bulk viscosity, frictional viscosity, frictional pressure, and granular temperature.

Regarding the modulus of elasticity ($G(\varepsilon_\beta)$) on the solids pressure (∇P_σ), the model considers the

data of Mutsers and Rietma.^[31] This model was selected since the experiments, and therefore the derivation of the Ettehadieh sub-model, were conducted for spherical particles. Also, as reported by Mutsers and Rietma,^[31] it was observed that the modulus of elasticity does not show a strong dependence on the mean particle diameter, but does show important variations when there is a large spread in particle diameter distribution (i.e., when there is the presence of fines), which is adequate for the experimental setup reproduced in this work, since $D_{\sigma, min} - \langle D_\sigma \rangle \cong 65 \mu\text{m}$:

$$G(\varepsilon_\beta) = -10^{-10.46\varepsilon_\beta + 6.577} \quad (5)$$

Even though the sub-model described by Equation (5) is an empirical expression included in the solids momentum transport equation (Equation (4)), it should be noted that the modulus of elasticity does have a theoretical background, and is included to account for the particle-particle interactions.^[30]

The second sub-model included is a volumetric momentum exchange term, the drag force (\mathbf{F}_d), which is described by Equation (6). This term accounts for the multiphase interactions ($\sigma - \beta$ interactions) and assumes that the drag force acting on the disperse phase is equal to the drag force on the continuous phase but in the opposite direction ($\mathbf{F}_{d,\beta} = -\mathbf{F}_{d,\sigma}$). This momentum exchange term consists of an interaction coefficient ($K_{\sigma\beta}$) multiplied by the slip velocity of the phases ($\mathbf{v}_{slip} = \mathbf{v}_\sigma - \mathbf{v}_\beta$). The interaction coefficient is modelled according to the sub-model reported by Gidaspow,^[32] which includes a drag coefficient (C_D). In the implemented Gidaspow model formulation, this drag coefficient is estimated according to the observations of Schiller and Naumann.^[33] The interaction coefficient and the drag coefficient are described by Equations (7) and (8), respectively, where the particle Reynolds Number is described by Equation (9):

$$\mathbf{F}_d = K_{\sigma\beta} (\mathbf{v}_\sigma - \mathbf{v}_\beta) = K_{\sigma\beta} \mathbf{v}_{slip} \quad (6)$$

$$K_{\sigma\beta} = \begin{cases} \frac{3\varepsilon_\beta\varepsilon_\sigma\rho_\beta C_D}{4D_\sigma} |\mathbf{v}_{slip}| \varepsilon_\beta^{-2.65} & \text{for } \varepsilon_\beta > 0.8 \\ 150 \frac{\mu_\beta \varepsilon_\sigma^2}{\varepsilon_\beta D_\sigma^2} + 1.75 \frac{\varepsilon_\sigma \rho_\beta}{D_\sigma} |\mathbf{v}_{slip}| & \text{for } \varepsilon_\beta < 0.8 \end{cases} \quad (7)$$

$$C_D = \begin{cases} 0.44 & \text{for } Re_p > 1000 \\ \frac{24}{Re_p} (1 + 0.15 Re_p^{0.687}) & \text{for } Re_p < 1000 \end{cases} \quad (8)$$

$$Re_p = \frac{\rho_\beta D_\sigma |\mathbf{v}_{slip}|}{\mu_\beta} \quad (9)$$

Finally, a third implemented sub-model is included to estimate an effective viscosity of the solid pseudo-phase. As suggested by Gidaspow,^[32] this sub-model is described by Equation (10), and is included for numerical robustness:

$$\mu_{eff} = \frac{\varepsilon_\sigma}{2} \quad (10)$$

The model described by Equations (1)–(4) is set to the following boundary conditions:

$$-\mathbf{n} \cdot \mathbf{v}_\beta = f(t)f(r) \langle V_\beta \rangle_0 (inlet) \quad (11)$$

$$\mathbf{v}_\sigma = 0 (inlet) \quad (12)$$

$$\varepsilon_\sigma \mathbf{v}_\sigma \cdot \mathbf{n} = 0 (inlet) \quad (13)$$

$$\varepsilon_\sigma \left[-\nabla P + \mu_\beta \left(\nabla \mathbf{v}_\beta + (\nabla \mathbf{v}_\beta)^T - \frac{2}{3} (\nabla \cdot \mathbf{v}_\beta) \mathbf{I} \right) \right] \mathbf{n} = 0 (outlet) \quad (14)$$

$$P = P_0 (outlet) \quad (15)$$

$$\mathbf{v}_\beta = 0 (walls) \quad (16)$$

$$\mathbf{v}_\sigma = 0 (walls) \quad (17)$$

$$\varepsilon_\sigma \mathbf{v}_\sigma \cdot \mathbf{n} = 0 (walls) \quad (18)$$

where \mathbf{n} is the normal vector to the surface of the prescribed boundary. In these boundary conditions, Equations (11)–(13) indicate that the inlet is pure air; Equations (14) and (15) indicate that there is no viscous stress of the continuous phase (β – phase) at the outlet, and that the pressure is atmospheric, respectively; and Equations (16)–(18) indicate that a no-slip boundary

condition is considered for both phases at the walls. It can be pointed out that, unlike other formulations based on the KTGF approach, this model does not include another sub-model or require any closure parameters to model the wall interactions, such as a particle-wall restitution coefficient or a specular coefficient.^[34] This allows to keep to the reduced number of coupled sub-models. However, it should be recognized that modelling the solids-wall and gas-wall interaction through a no-slip boundary condition is an approximation, and that this model does not include a fully resolved wall interaction model. Nevertheless, as will be shown in the results, the model exhibits a high predictive quality to reproduce the near-wall phenomena measured experimentally.

It can be seen that the average superficial air inlet velocity (Equation (11)) is multiplied by two functions, one dependent on the time and one dependent on the radial position, $f(t)$ and $f(r)$, respectively. The time function ($f(t)$) is a smoothed ramp function from $t = 0$ to $t = 2 \times 10^{-3}$ s, which is included to mimic the start-up of the system. That is, $f(t)$ only affects the inlet boundary condition during the interval of $0 \leq t \leq 2 \times 10^{-3}$ s. At $t > 2 \times 10^{-3}$ s, $f(t) = 1$. The radial position function ($f(r)$) is a function that indicates that the air inflow at the inlet boundary is not homogeneous through all the surfaces. With this function, the inflow profile can be assumed to be similar to that of a fully developed flow, by virtue of the distribution achieved on the plenum region. That is, $f(r) = 1 - \left(\frac{r}{R_C}\right)^2$. The product of these functions with the average inlet velocity ($f(t)f(r) \langle V_\beta \rangle_0$) satisfies the constraint set on Equation (19), which indicates that the average of the superficial air inlet velocity on the boundary at times $t \geq 2 \times 10^{-3}$ s is equal to the average superficial air velocity indicated in Table 1:

$$\frac{1}{A_{inlet}} \int_{A_{inlet}} -\mathbf{n} \cdot \mathbf{v}_\beta dA \Big|_{at t \geq 2 \times 10^{-3} s} = \langle V_\beta \rangle_0 \quad (19)$$

It can be noted that the implemented model has the following underlying assumptions:

1. The solids transport is mainly due to the advection, and thus $\mathbf{O}(\mathbf{v}_\sigma \nabla \cdot \mathbf{v}_\sigma) \gg \mathbf{O}(\nabla \cdot \boldsymbol{\tau}_\sigma)$.
2. The strain-tensor contributions that describe the interaction between the solids can be separated into two contribution, modelled by a solids pressure sub-model (∇P_σ), by virtue of Equations (20) and (21),^[30,35] plus an effective molecular/viscous interaction term:

$$\begin{aligned} \nabla \cdot \boldsymbol{\tau}_\sigma &= \frac{\partial \tau_{xx}}{\partial \varepsilon_\beta} \frac{\partial \varepsilon_\beta}{\partial x} + \frac{\partial \tau_{yy}}{\partial \varepsilon_\beta} \frac{\partial \varepsilon_\beta}{\partial y} + \frac{\partial \tau_{zz}}{\partial \varepsilon_\beta} \frac{\partial \varepsilon_\beta}{\partial z} \\ &= \sum_i \frac{\partial \tau_{ii}}{\partial \varepsilon_\beta} \frac{\partial \varepsilon_\beta}{\partial i} = \nabla \varepsilon_\beta \end{aligned} \quad (20)$$

$$\sum_i \frac{\partial \tau_{ii}}{\partial \varepsilon_\beta} = -G(\varepsilon_\beta) \quad (21)$$

3. The elasticity module ($G(\varepsilon_\beta)$) required to provide closure to the solids pressure sub-model can be estimated by the empirical expression proposed by Ettehadieh et al.^[30]
4. The multiphase interactions can be properly estimated by a drag force sub-model based on the one proposed by Gidaspow.^[32]
5. The interaction between the air and walls, and solids and walls, can be described by no-slip boundary conditions.

It is important to highlight that a model with these characteristics requires only the inclusion of three sub-models. Hence, its applicability could be restrained to the applicability of these sub-models selected to give closure to the solid-solid interactions and the solids-fluid interactions. This represents a remarkable advantage of the implemented model in this work in comparison with other models found in the literature, which require a vast number of sub-models. However, the implemented model in this work does not allow for the evaluation of parameters related to the bubble geometry, such as bubble size and bubble frequency, nor the parameters related to the cluster formation and growth since the actual solids-air interphase is not predicted. Despite this, as will be shown in the results, the model possesses a high predictive quality in terms of local radial profiles, such as solids holdup, solids velocity, and pressure drop.

For all tested cases, the considered time was 10 s with time steps of $\Delta t = 1 \times 10^{-3}$ s. Preliminary tests considering longer times were conducted; however, it was found that there were no significant differences in the predicted fields when considering longer times for the time averaging. Furthermore, the magnitude of the considered time is in agreement with other works found in the literature.^[17,19,36] Time-averaged profiles were estimated ($\langle \psi \rangle_t = \frac{1}{t_{total} - 3s} \int_{3s}^{t_{total}} \psi dt; \psi = \text{any field variable}$) ignoring the initial 3 s due to start-up effects. In the preliminary tests it was also determined that for all the tested cases, the start-up effects were mostly present during the initial 3 s. However, it should be pointed out that under different conditions, such start-up effects might extend for longer times, and hence the integration bounds would need to be modified.

3 | EXPERIMENTAL STUDY

3.1 | Experimental setup

The experimental setup used to validate the predictive quality of the implemented model corresponds to the

setup reported by Taofeeq et al. in previous contributions.^[1,8,13–15] The setup consisted of a Plexiglass column with internal diameter of $D_C = 14$ cm, and a height of $L_C = 184$ cm, packed Geldart B type glass beads of an average diameter of $\langle D_\sigma \rangle = 365 \mu\text{m}$, and a density of $\rho_\sigma = 2500 \frac{\text{kg}}{\text{m}^3}$. Details of the experimental setup are shown on Figure 1.

Experiments were conducted at superficial gas inlet velocities between $\langle V_\beta \rangle_0 = 0.15 - 1.1 \frac{\text{m}}{\text{s}}$, in order to cover all the different flow regimes (packed bed, bubbling, slugging, and turbulent), as reported in our previous contribution.^[1] From this range of superficial inlet velocities, cases within the bubbling and slugging flow regime were selected in order to conduct a detailed experimental study to determine the local radial solids holdup, velocities and local pressure drops. The selected cases corresponded to relative gas inlet velocities of $\left(\frac{\langle V_\beta \rangle_0}{V_{mf}} \right)$ 1.6, 1.76, 1.96 and 2.14. Where the minimum fluidization velocity was found to be $V_{mf} = 0.4 \frac{\text{m}}{\text{s}}$, according to the experimental observations.^[13,14] Further details of the operation conditions and a summary of the geometrical characteristics of the setup are shown in Table 1.

3.2 | Measurement techniques

An advanced optical fibre probe was used to measure the local key hydrodynamic parameters. Optical probes have been widely used in several experimental studies reported in the literature.^[37–40] However, the commonly used optical probes cannot simultaneously measure the solids concentration and velocities.^[41–43] In order to overcome this major drawback, a new generation of sensors has been continuously developed through the last decades.^[43,44] Despite such developments, simultaneously measuring the solids holdup and velocity with a high accuracy and time resolution has been a challenge. In our laboratory, we developed a data and signal processing algorithm to simultaneously obtain highly accurate time-resolved solids holdup and velocities, using an optical probe manufactured according to our specifications. This new probe was manufactured by the Institute of Process Engineering of the Chinese Academy of Sciences, and consisted of two sub-probes, with a dimension of 3 mm in diameter. The major difference in the developed probe consists in the arrangement of these two sub-probes that contained several layers of light emitting and receiving layers of small optical fibres. Each of these sub-probes has a diameter of 1 mm and are separated 1 mm from each other. The development, calibration, and processing of the registered signals of the optical fibre probe has been discussed in

previous contributions.^[14,15] Radial solids holdup, solids velocity profiles, and other bubble hydrodynamic characteristics, at three different bed height locations, ($\frac{z}{D_c} = 0.75, 1.5, 2.0$) were measured. Details of these locations can be seen in Figure 1.

A differential pressure transducer was used in order to obtain the radial local pressure drop profile and the overall pressure drop for the different tested cases. Locations for the pressure transducer probe were selected to be at 4.5 cm and 30.5 cm from the distribution plate.

Coupling these measurement techniques in the experimental setup allowed reliable benchmarking data of the key macroscopic solid dynamics parameters (overall pressure drop and overall holdup) and detailed radial solids holdup, velocity, and local pressure drop profiles to be obtained. Such information allowed for the validation of the macroscopic and local predictions of the implemented model. Nevertheless, it should be kept in mind that the validation of the model, as will be presented in the following section, corresponds to a practical validation, rather than a full validation.^[45] This means, that the model exhibits a high accuracy in the predictions and can be reliable for studying unexplored conditions, as long as the intended extrapolation conditions are not highly dissimilar to the tested conditions. In fact, in general terms, a model can only be claimed to be validated under the limitations, assumptions, and conditions that have been tested for its validation; and thus, its applicability with confidence on the accuracy of its predictions is considered to be constrained to similar conditions. For this case, it can be considered that the model is constrained to fluidized beds packed with Geldart B particles, operating under bubbling and slugging conditions.

In this sense, in a recent contribution by our research group,^[46] we implemented a similar mathematical model as the one proposed in this work for a spouted bed packed with Geldart D particles. Despite that the general E2P model followed the same model described by Equations (1)–(4), the coupled sub-models for the drag force and the modulus of elasticity required to be modified to be applicable for Geldart D particles. In this contribution, the model exhibited a high accuracy in the predictions of experimentally measured solids holdup profiles under different inlet velocities, particle sizes, and static bed heights. This shows that the model has high flexibility to be adaptable for different gas-solid systems, and that it can provide highly accurate predictions as long as it is coupled with suitable sub-models. In this sense, the fact that only two sub-models need to be selected in order to enable the application of the model for different gas-solid systems can be considered an important advantage.

4 | RESULTS AND DISCUSSION

4.1 | Validation of the macroscopic parameters

Predicted and experimentally measured overall pressure drops can be seen in Figures 6 and 7. Figure 6 shows the time series of the predicted pressure drop by the model. This time series is evaluated as described by Equation (22), where A_T is the transversal area of the column. In these time series it can be seen that an important effect of the start-up is present during the first second of the considered time, and that at larger times this effect is diminished, even though the fluctuations are always present. The coefficient of variation ($CoV = \frac{\sigma_{\psi,t}}{\langle \psi \rangle_t}$) of the predicted time series pressure drop is also shown in Figure 6 for the different inlet dimensionless velocity cases. The estimated values of the CoV suggest that the considered time for the simulations is large enough, and thus the evaluated time-averaged profiles can be representative of the steady state operation of the column:

$$\langle \Delta P \rangle = \frac{1}{A_T} \int_{A_T} PdA \Big|_{z=4.5} - \frac{1}{A_T} \int_{A_T} PdA \Big|_{z=30.5} \quad (22)$$

Figure 7 shows the time-averaged overall pressure drop from Figure 6 in comparison with the experimentally determined pressure drop. In both series from Figure 7, the error bars represent the time SD ($\sigma_{\psi,t}$). It can be seen

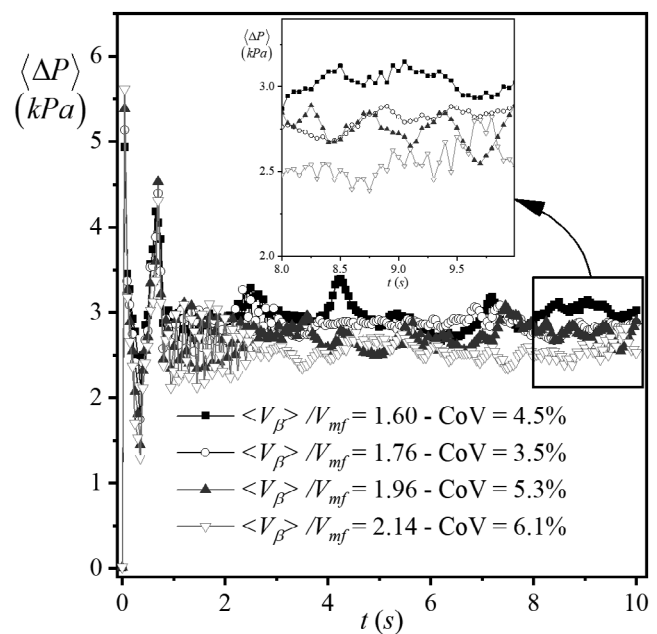


FIGURE 6 Average pressure drops time series for the different tested cases

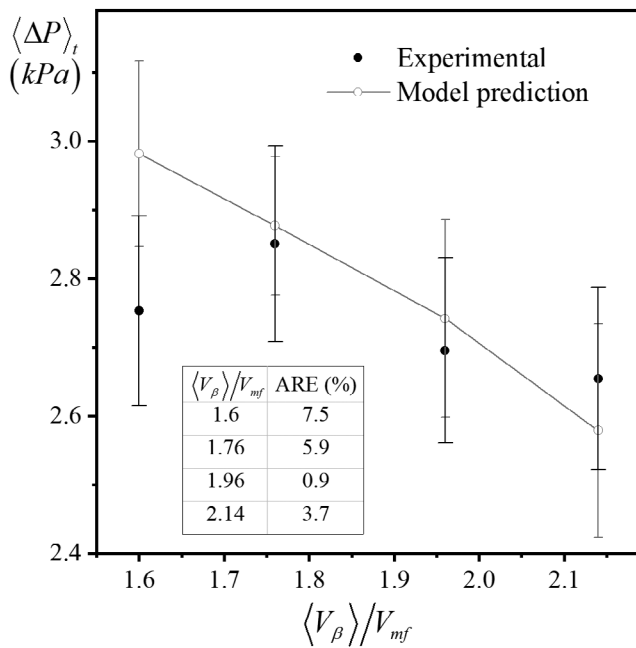


FIGURE 7 Predicted and experimentally determined time-averaged overall pressure drop at different dimensionless inlet velocities

that there is a good agreement in the predicted pressure drop at the different inlet velocities, despite a higher deviation being observed for the case of $\langle V_\beta \rangle_0 = 1.6$. Nevertheless, the absolute relative error ($ARE = \frac{|\psi_{EXP} - \psi_{CFD}|}{\psi_{EXP}}$) for this case is of only 7.5%.

Figure 8 shows a comparison between the experimentally measured and model predictions of the time-averaged overall gas holdup ($\langle \varepsilon_\beta \rangle_t$), for superficial gas inlet velocities between 0.4–1.0 m/s. This velocity range covers bubbling and slugging flow regimes, according to our previous studies. In Figure 8, it can be seen that the predictions for the values and the trends of the overall gas holdup is in close agreement with the experimental measurements. In these, the average absolute relative error ($AARE = \sum_{i=1}^n \frac{|\psi_{EXP,i} - \psi_{CFD,i}|}{\psi_{EXP,i}}$) was estimated to be 5.2%.

Figures 7 and 8 suggest that the model has a high accuracy in the prediction of these two key macroscopic hydrodynamics parameters in the fluidized bed. These two parameters are essential for scale-up and design tasks of fluidized beds, and thus, a model capable of reliably predicting such parameters is desirable. However, the mathematical model for the fluidized bed cannot be claimed to be validated merely by the comparison of the macroscopic parameters. In order to provide a more comprehensive validation of the implemented model, in the following sub-section, the comparison of the local predictions and measurements is presented.

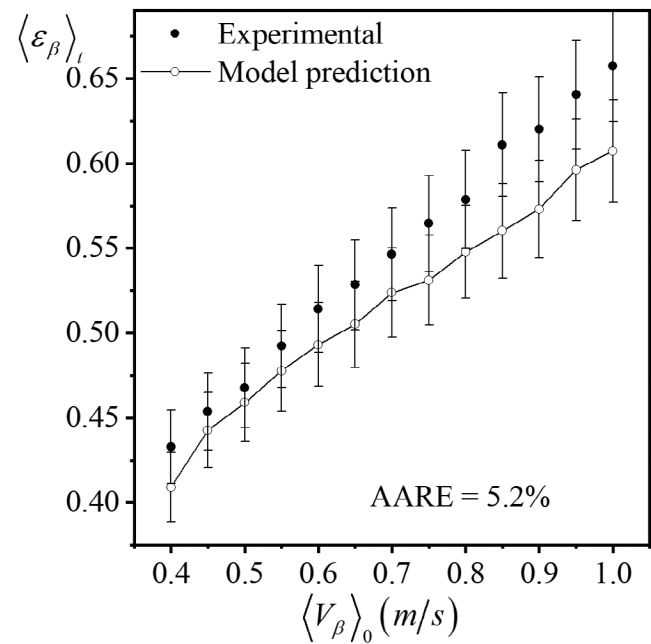


FIGURE 8 Predicted and experimentally determined time-averaged overall gas holdup profiles at different inlet velocities

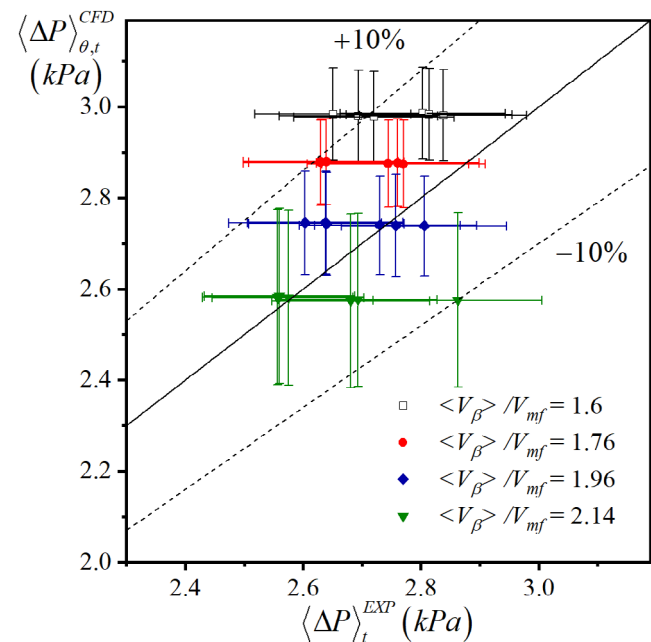


FIGURE 9 Parity plot of the predicted and experimentally determined time-averaged local pressure drop for different dimensionless inlet velocities

4.2 | Validation of the local profiles

The experimental measurements from the optical fibre probes and the differential pressure transducer probe allowed the radial profiles of the solids holdup, solids velocity, and local pressure drop to be determined, as reported in previous contributions.^[13,14] These profiles,

however, correspond to measurements in the radial direction at a single angular position, and thus, overlook the asymmetric behaviour that might be present in the bed. In order to properly compare with the predictions of the implemented model, it is convenient to compare the measurements with the predicted profiles averaged on the angular direction. This means that the following reported radial profiles from the model correspond to radial profiles averaging the asymmetry of the different angular positions ($\langle \psi \rangle_{\theta} = \frac{1}{2\pi} \int_0^{2\pi} \psi d\theta$); for time-averaged

profiles, the angle and time averaging of the field is considered to be ($\langle \psi \rangle_{\theta,t} = \frac{1}{2\pi(t_{total} - 3s)} \int_0^{2\pi} \int_{3s}^{t_{total}} \psi d\theta dt$).

A comparison between all measured radial positions for the cases shown in Figure 7 and the corresponding predictions by the implemented model can be seen in the parity plot shown in Figure 9. In this, the dashed lines represent deviations of $\pm 10\%$. It can be seen that for all tested cases, the deviations from the predictions are within $\pm 10\%$. Results from Figures 7 and 9 suggest a good predictive quality of the overall and local pressure drop by the implemented model.

Figure 10 shows a parity plot of the predicted time-averaged solids holdup ($\langle \varepsilon_{\sigma} \rangle_{\theta,t}$) against the experimental measurements at the three different axial locations of the bed ($\frac{z}{D_C} = 0.75, 1.5, 2.0$). In this, it can be seen that for all cases, the model overpredicts the solids holdup, with deviations in the majority of the predictions under 10%. The estimated AAREs are estimated to be 8.7%, 11.3%, 9.8% and 8.6% for $\frac{\langle V_{\beta} \rangle_0}{V_{mf}} = 1.6, 1.76, 1.96,$ and 2.14, respectively.

A comparison of the predicted and experimental local radial time-averaged solids holdup profile for the case of $\frac{\langle V_{\beta} \rangle_0}{V_{mf}} = 1.6$ can be seen in Figures 11A-C, for $\frac{z}{D_C} = 0.75, 1.5,$ and 2.0, respectively. It can be seen that for all three axial locations, the predicted profiles by the implemented model exhibit a good agreement in the trends. At the location closest to the distribution plate ($\frac{z}{D_C} = 0.75$), it can be noted that the model overpredicts the solids holdup in the region close to the column walls, while for the location at $\frac{z}{D_C} = 2.0$, a good agreement is shown in the region close to the wall, but overpredictions are seen in the centre of the column. In the middle location ($\frac{z}{D_C} = 1.5$), a constant overprediction can be observed. Similar behaviours are obtained for the other inlet

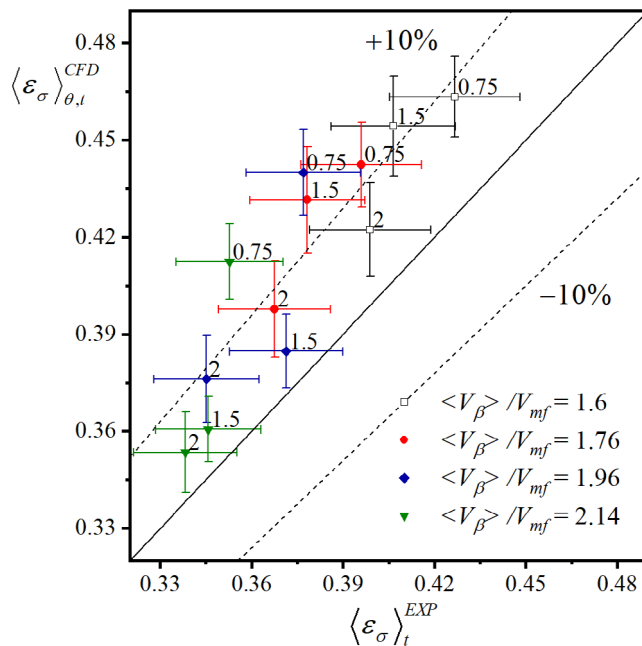


FIGURE 10 Parity plot of the predicted and experimentally determined time-averaged solids holdup at the different axial locations of the bed ($z/D_C = 0.75, 1.5, 2.0$) for all tested cases

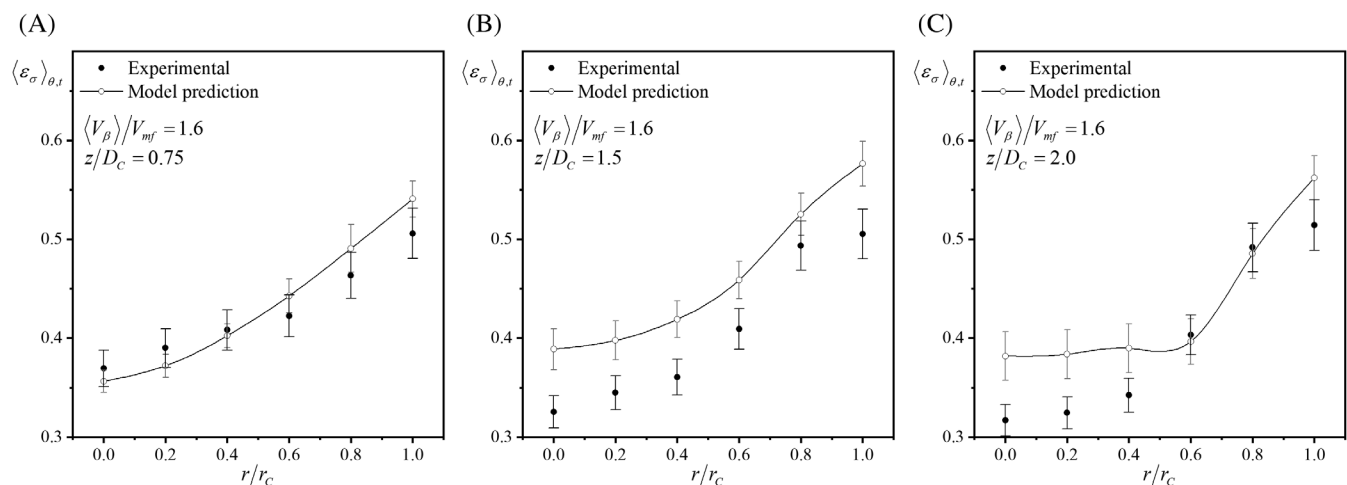


FIGURE 11 Predicted and experimentally determined radial solids holdup profile at (A) $z/D_C = 0.75$, (B) $z/D_C = 1.5$, and (C) $z/D_C = 2.0$ for the inlet dimensionless velocity $\langle V_{\beta} \rangle_0 / V_{mf} = 1.6$

velocities cases. Despite these observed deviations, when estimating the root mean squared deviation ($RMSD = \left[\sum_{i=1}^n (\psi_{EXP,i} - \psi_{CFD,i})^2 \right]^{0.5}$) for all velocity cases at all the axial positions, deviations are found to be under 5%. A summary of the obtained RMSD for the predictions of the solids holdup is shown in Table 2. These results suggest that the implemented model also has a high predictive quality for the overall and local time-averaged solid holdups predictions. To a certain extent, such deviations observed in the near-wall region might arise from the assumption made on the wall boundary condition. The inclusion of a sub-model for the wall interactions might improve the predictions for such regions, however, it would add further uncertainty for extrapolation studies, as previously discussed.

Similar to Figures 11A–C, Figures 12A–C show a sample of the predicted and experimentally determined solids velocity profiles for the case of $\frac{\langle V_\beta \rangle_0}{V_{mf}} = 1.96$ for $\frac{z}{D_c} = 0.75, 1.5,$ and $2.0,$ respectively. In these, the axial component of the predicted velocity profile ($v_{\sigma,z}$) is shown for a proper comparison with the experimental

TABLE 2 Root mean squared deviation (RMSD) of time-averaged solids holdup profile predictions

$\frac{z}{D_c}$	$\frac{\langle V_\beta \rangle_0}{V_{mf}}$			
	1.6	1.76	1.96	2.14
0.75	2.2%	4.8%	4.3%	5.8%
1.5	5.6%	3.7%	2.8%	3.3%
2.0	4.5%	5.2%	4.0%	5.3%
$\langle RMSD \rangle$	4.1%	4.6%	3.7%	4.8%
$\langle RMSD \rangle = \sum_{i=1}^n \frac{RMSD_i}{n}$				

measurements. From Figure 12, it can be seen that the predicted trends from the implemented model exhibit a fairly good agreement with the experimental measurements, despite local deviations being observed. For the case shown in Figure 12A ($\frac{z}{D_c} = 0.75$), it is observed that both the trend and the local values are in agreement between the experiments and the model predictions. On the other axial positions (Figure 12B,C), it can be seen that the model predicts higher velocities in the centre of the column, and back-mixing in the wall regions. A nearly perfect agreement is observed in the prediction of the back-mixing region close to the wall. Similar observations can be pointed out for the other velocity cases.

A comparison of the predicted time-averaged solids velocity profiles for all cases at all the radial and axial locations can be seen in the parity plot shown in Figure 13. From Figure 13, it can be seen that high deviations ($ARE \geq 20\%$) are found between the experimental and the model predictions. It can be noted that the model, in most cases, overpredicts the velocity profiles, and that the model properly predicts the regions of back-mixing, despite the deviation in the velocity magnitude.

In order to properly compare the predictions with the experimental measurements, Table 3 shows the RSMD for all velocity cases at all axial positions. In these results, it can be seen that for all cases the RSMD is under 22%, with an average $\langle RMSD \rangle$ down to 11.8% for the case of $\frac{\langle V_\beta \rangle_0}{V_{mf}} = 1.6$. These values of RSMD could be considered to be within an acceptable range and would imply that despite deviations being in the predictions, there is, to a certain extent, an agreement in the predicted trends.

A source of the observed deviations in the compared time-averaged fields (solids holdup, solids velocity, and pressure drop) can be attributed to systematic effect of the measurement technique that is not fully captured by

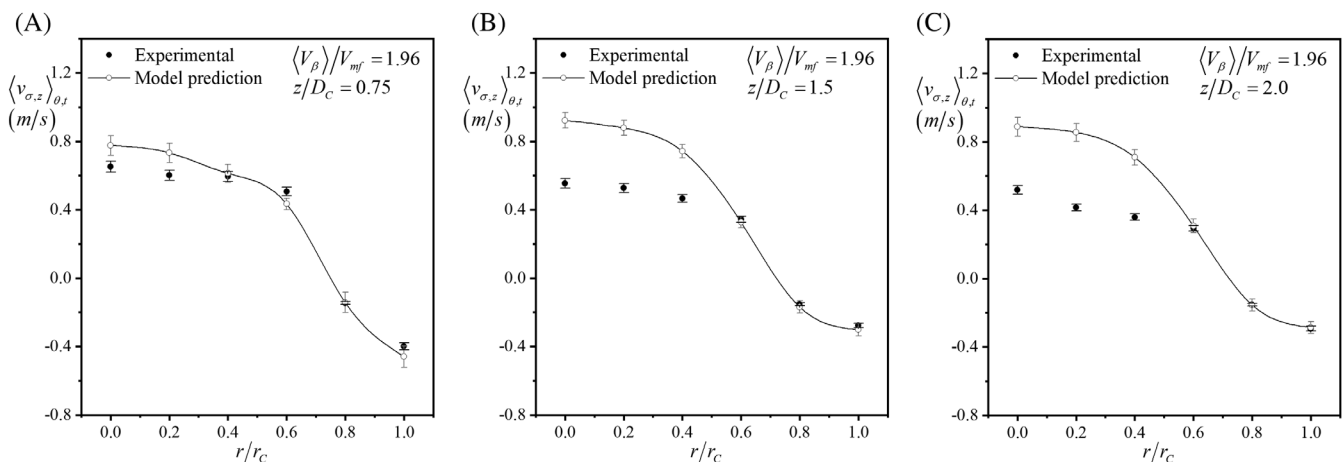


FIGURE 12 Predicted and experimentally determined radial solids velocity profile at (A) $z/D_c = 0.75,$ (B) $z/D_c = 1.5,$ and (C) $z/D_c = 2.0$ for the inlet dimensionless velocity $\langle V_\beta \rangle_0 / V_{mf} = 1.96$

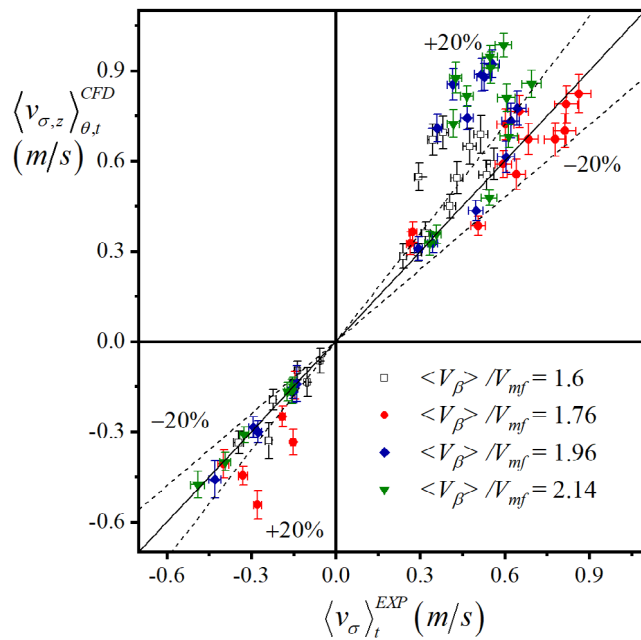


FIGURE 13 Parity plot of the predicted and experimentally determined time-averaged solids velocity for all radial and axial location on the tested cases

TABLE 3 Root mean squared deviation (RMSD) of time-averaged solids velocity profile predictions

$\frac{z}{D_c}$	$\frac{\langle V_{\beta} \rangle_{\theta}}{V_{mf}}$			
	1.6	1.76	1.96	2.14
0.75	2.3%	8.3%	7.6%	11.3%
1.5	11.8%	21.2%	23.7%	26.8%
2.0	21.3%	26.0%	27.4%	26.6%
(RMSD)	11.8%	18.5%	19.6%	21.6%

the implemented model. Despite the implemented measurement technique having a validated precision in its measurements,^[15] it should be considered that this is an invasive technique, and can thus have an unmeasured effect on the phenomena in its surroundings. In the implemented simulations, the effect that the immersed probe could cause is not incorporated. Despite the probe having small dimensions, mathematically in the model this would represent a local source of non-linearities due to the wall-solids and wall-air interactions through the probe surface.

Another possible source of such deviations can be attributed to limitations in the incorporated sub-models. From Tables 2 and 3, it can be seen that the deviations in the model predictions increase as the superficial inlet velocity increases. In this regard, it should be noted that the solids pressure sub-model was developed by

macroscopic/overall pressure drop and solids holdup experimental measurements,^[31] and thus overlooks the local scale interaction phenomena. That is, in order to improve the model predictive quality of the local scale phenomena, an enhanced solids pressure sub-model must be developed with a mechanistic or phenomenological approach considering the local scale phenomena, therefore overcoming the empirical nature of the currently available solids pressure sub-models. Nevertheless, it should be noted that the model discussed in this work has the flexibility of incorporating other solids pressure models with enhanced predictive quality, and is suitable for different systems. This was observed in our recent contribution where this model was adapted for a spouted bed packed with Geldart D particles, and a similar high predictive quality was obtained.^[46]

The evaluated deviations in the fields could also be attributed to the asymmetrical behaviour of the fluidized bed. Figure 14 shows a snapshot of the predicted local solids holdup profiles at the three considered axial locations ($\frac{z}{D_c} = 0.75, 1.5, 2.0$) and at the inlet, at time $t = 9$ s for the four considered inlet velocities. Figure 14 clearly shows that the predicted fields for all cases are asymmetric. Furthermore, it can be seen that the distribution of the solid phase is highly affected by the inlet velocity. This effect is not only on the overall values of the field, but on the distribution of the field on the radial and axial locations (i.e., bubbles distribution). This phenomena has been acknowledged in the literature^[8,14,19,25,32], however, in the experimental measurements, only a radial distribution in one angular position was measured. This implies that the fields used for comparison and validation of the implemented model do not properly consider the asymmetry of the phenomena and thus could explain the evaluated deviations. Nevertheless, it is important to note that the experimental measurements considered sampling times between 65–160 s, which is large enough to capture, to a great extent, the chaotic behaviour of the momentum transfer phenomena.

5 | REMARKS

Simulations for a fluidized bed system experimentally studied in previous contributions were conducted. The implemented model considered an E2P approach, with three closures for the multiphase and multiscale interactions. Experimentally determined local solids holdup, solids velocity, and pressure drop were compared against the model predictions, in order to validate the predictive quality of the implemented model. The following results were found:

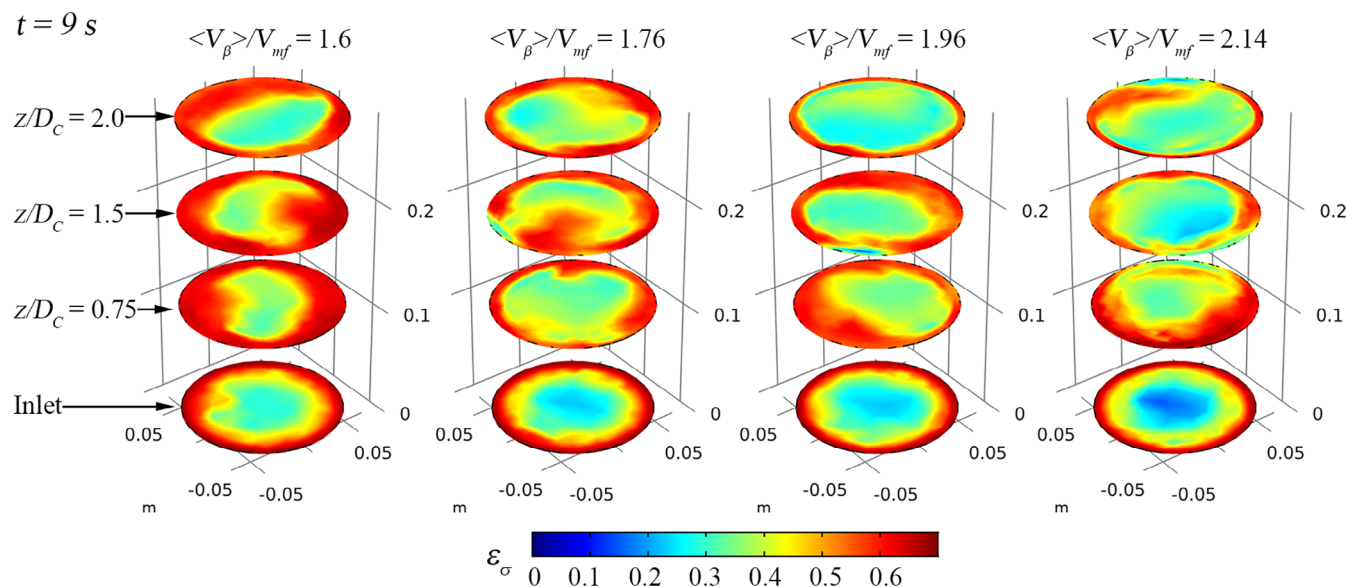


FIGURE 14 Predicted local solids holdup profile at the three considered axial locations ($z/D_C = 0.75, 1.5, 2.0$) for the different dimensionless inlet velocities at $t = 9$ s

- Pressure drop was predicted with an AARE between 8.6%–11.3%.
- Local solids holdup profiles were predicted with an RMSD under 5% for all the tested cases at all the compared locations inside the bed.
- Solids velocity was predicted with an RMSD between 2.3%–27.4% for all the tested cases at all the compared locations inside the bed.

The obtained predictions, when compared with the experimental measurements, suggest a high and consistent predictive quality of the implemented model. This can be clearly observed in the constant overprediction of the local solids holdups and local solids velocity by the model. The predictive quality of the model can be attributed to two main factors: (i) the model considers the multiphase and multiscale interaction through the inclusion of few sub-models, which results in a robust model with a broad range of applicability (i.e., the applicability of the model is only limited by these sub-models' valid conditions) and (ii) the experimental advanced measurement techniques allowed local key hydrodynamic parameters profiles to be measured, and thus allowed the model predictions of the local phenomena to be properly compared, rather than with macroscopic parameters. These two characteristics of the present study represent a paramount advantage in comparison with other works reported in the literature.^[17,19,26]

The implemented model, with the discussed characteristics and limitations, has the capability for extrapolation studies, such as optimization and scale-up studies

aided by the model, for fluidized bed systems packed with Geldart B particles operating under bubbling or slugging flow regimes. Further comparison to validate the predictive quality of the model for a different kind of solids particle packing and the effect of immersed vertical internals is still required. It should be noted that the model has the advantage of having a high flexibility to be adapted for different systems, provided that suitable sub-models are selected, as shown in our recent contribution.^[46] In this sense, the inclusion of a reduced number of sub-models can be considered as an advantage that enhances the flexibility of the model, as only two sub-models need to be selected in order to enable the application of the model for a different gas-solid system. A new solids pressure model, which is developed considering the local multiphase interaction phenomena and that has a mechanistic or phenomenological basis, must be developed in order to overcome the empirical nature of the available modulus of elasticity sub-models, and therefore, to enhance the predictive quality of the model.

ACKNOWLEDGEMENTS

The authors (SU) would like to thank the Multiphase Flow and Reactors Engineering and Education Laboratory (mFReel) for the provided support and funding.

NOMENCLATURE

<i>ARE</i>	Absolute relative error
<i>AARE</i>	Average absolute relative error
<i>AD</i>	Absolute deviation
A_i	Area of section i
<i>CFD</i>	Computational fluid dynamics

CoV	Coefficient of variation
D_C	Column diameter (m)
D_σ	Solid particle diameter (m)
$E2P$	Euler-two-phase
F_d	Volumetric drag force (N/m ³)
$G(\varepsilon_\sigma)$	Elasticity coefficient
L_C	Column length
P	Pressure (Pa)
R_C	Column radius (m)
RMSD	Root Mean squared deviation
V_i	Superficial velocity of phase i (m/s)
\mathbf{v}_i	Superficial velocity vector of phase i (m/s)
\mathbf{v}_{slip}	Slip velocity (m/s)
\mathbf{v}_{ij}	j component of the superficial velocity vector of phase i (m/s)

Super/subscripts and averages

CFD	Model prediction
EXP	Experimentally determined quantity
mf	Minimum fluidization
0	Initial conditions
$total$	Total measuring time

Average quantities

$\langle \rangle$	Average quantity
$\langle \rangle_t$	Time-averaged quantity
$\langle \rangle_\theta$	Angle-averaged quantity
$\langle \rangle_{\theta,t}$	Angle and time-averaged quantity

Greek symbols

β	Gas phase
ε_i	Volume fraction (holdup) of phase i
μ_i	Dynamic viscosity of phase i (Pa s)
ρ_i	Density of phase i (kg/m ³)
σ	Solid pseudo-phase
$\sigma_{\psi,t}$	Time SD of variable ψ
τ_σ	Solid stress strain-tensor (N/m ³)
ψ	Any field variable

PEER REVIEW

The peer review history for this article is available at <https://publons.com/publon/10.1002/cjce.24070>.

ORCID

Sebastián Uribe <https://orcid.org/0000-0001-8527-8455>

REFERENCES

- [1] H. Taofeeq, M. Al-Dahhan, *Chem. Eng. Res. Des.* **2018**, 138, 87.
- [2] J. Arnaldos, J. Casal, *Powder Technol.* **1996**, 86, 285.
- [3] C. Higman, S. Tam, *Chem. Rev.* **2014**, 114, 1673.
- [4] H. Zhong, J. Zhang, S. Liang, Y. Zhu, *Particul. Sci. Technol.* **2019**, 0, 1.
- [5] A. Efthaima, *PhD Thesis*, Missouri University of Science and Technology, Rolla, MO **2016**.
- [6] F. Zaid, *PhD Thesis*, Missouri University of Science and Technology, Rolla, MO **2013**.
- [7] A. Bisio, R. L. Kabel, *Scaleup of Chemical Processes: Conversion from Laboratory Scale Tests to Successful Commercial Size Design*, Wiley, New York **1985**.
- [8] H. Taofeeq, M. Al-Dahhan, *Chinese J. Chem. Eng.* **2018**, 26, 1401.
- [9] S. Maurer, D. Gschwend, E. C. Wagner, T. J. Schildhauer, J. Ruud van Ommen, S. M. A. Biollaz, R. F. Mudde, *Chem. Eng. J.* **2016**, 298, 17.
- [10] A. Acosta-Iborra, C. Sobrino, F. Hernández-Jiménez, M. de Vega, *Chem. Eng. Sci.* **2011**, 66, 3499.
- [11] G. C. Brouwer, E. C. Wagner, J. R. van Ommen, R. F. Mudde, *Chem. Eng. J.* **2012**, 711, 207.
- [12] F. Schillinger, T. J. Schildhauer, S. Maurer, E. Wagner, R. F. Mudde, J. R. van Ommen, *Int. J. Multiphas. Flow* **2018**, 107, 16.
- [13] H. Taofeeq, M. H. Al-Dahhan, *Can. J. Chem. Eng.* **2018**, 96, 2185.
- [14] H. Taofeeq, M. Al-Dahhan, *Adv. Powder Technol.* **2018**, 29, 2548.
- [15] H. Taofeeq, S. Aradhya, J. Shao, M. Al-Dahhan, *Flow Meas. Instrum.* **2018**, 63, 18.
- [16] X. Lan, C. Xu, J. Gao, M. Al-Dahhan, *Chem. Eng. Sci.* **2012**, 69, 419.
- [17] T. Wang, Z. Xia, C. Chen, *Chem. Eng. Sci.* **2019**, 202, 208.
- [18] F. Vejahati, N. Mahinpey, N. Ellis, M. B. Nikoo, *Can. J. Chem. Eng.* **2009**, 87, 19.
- [19] V. Verma, T. Li, J. F. Dietiker, W. A. Rogers, *Chem. Eng. J.* **2016**, 287, 727.
- [20] V. Agrawal, Y. Shinde, M. T. Shah, R. P. Utikar, V. K. Pareek, J. B. Joshi, *Adv. Powder Technol.* **2018**, 29, 2658.
- [21] D. Liu, B. van Wachem, *Powder Technol.* **2019**, 343, 145.
- [22] X. Ku, T. Li, T. Løvås, *Chem. Eng. Sci.* **2015**, 122, 270.
- [23] D. Jajcevic, E. Siegmann, C. Radeke, J. G. Khinast, *Chem. Eng. Sci.* **2013**, 98, 298.
- [24] F. Alobaid, J. Ströhle, B. Epple, *Adv. Powder Technol.* **2013**, 24, 403.
- [25] A. Busciglio, G. Vella, G. Micale, L. Rizzuti, *Chem. Eng. Sci.* **2010**, 65, 4782.
- [26] S. Hu, X. Liu, *Chem. Eng. J.* **2020**, 383, 123122.
- [27] J. Zhou, J. R. Grace, C. J. Lim, C. M. H. Brereton, *Chem. Eng. Sci.* **1995**, 50, 237.
- [28] J. Zhou, J. R. Grace, S. Qin, C. M. H. Brereton, C. J. Lim, J. Zhu, *Chem. Eng. Sci.* **1994**, 49, 3217.
- [29] H. Enwald, E. Peirano, A. Almstedt, *Int. J. Multiphas. Flow* **1996**, 22, 21.
- [30] B. Etehadieh, D. Gidaspow, R. W. Lyczkowski, *AIChE J.* **1984**, 30, 529.
- [31] S. M. Mutsers, K. Rietma, *Powder Technol.* **1977**, 18, 239.
- [32] D. Gidaspow, *Multiphase Flow and Fluidization: Continuum and Kinetic Theory Descriptions*, Academic Press, London, UK **1994**.
- [33] L. Schiller, Z. Naumann, *Z. Ver. Dtsch. Ing.* **1933**, 77, 318.
- [34] T. Li, J. Grace, X. Bi, *Powder Technol.* **2010**, 203, 447.
- [35] J. W. Pritchett, T. R. Blake, S. K. Garg, *AIChE Symp. S.* **1978**, 74, 134.

- [36] H. Zhong, Y. Zhang, Q. Xiong, J. Zhang, Y. Zhu, S. Liang, B. Niu, X. Zhang, *Powder Technol.* **2020**, 364, 363.
- [37] T. Pugsley, H. Tanfara, S. Malcus, H. Cui, J. Chaouki, C. Winters, *Chem. Eng. Sci.* **2003**, 58, 3923.
- [38] K. Dubrawski, S. Tebianian, H. T. Bi, J. Chaouki, N. Ellis, R. Gerspacher, R. Jafari, A. Kantzas, C. Lim, G. S. Patience, T. Pugsley, M. Z. Qi, J. X. Zhu, J. R. Grace, *Powder Technol.* **2013**, 235, 203.
- [39] S. Tebianian, K. Dubrawski, N. Ellis, R. A. Cocco, R. Hays, S. B. Reddy Karri, T. W. Leadbeater, D. J. Parker, J. Chaouki, R. Jafari, P. Garcia-Trinanes, J. P. K. Seville, J. R. Grace, *Chem. Eng. Sci.* **2015**, 127, 310.
- [40] M. Al-Dahhan, S. Aradhya, F. Zaid, N. Ali, T. Aljuwaya, *Procedia Engineer* **2014**, 83, 469.
- [41] Y. Matsuno, H. Yamaguchi, T. Oka, H. Kage, K. Higashitani, *Powder Technol.* **1983**, 36, 215.
- [42] M. Olazar, M. J. S. José, L. L. Ricardo, S. Alvarez, J. Bilbao, *Ind. Eng. Chem. Res.* **1995**, 34, 4033.
- [43] J. Liu, J. R. Grace, X. Bi, *AIChE J.* **2003**, 49, 1421.
- [44] Z. Wang, H. T. Bi, C. J. Lim, *Can. J. Chem. Eng.* **2009**, 87, 264.
- [45] J. R. Grace, F. Taghipour, *Powder Technol.* **2004**, 139, 99.
- [46] S. Uribe, B. Qi, O. Farid, M. Al-Dahhan, *Energies* **2020**, 13, 4738.

How to cite this article: Uribe S, Taofeeq H, Al-Dahhan M. Modelling and validation of a gas-solid fluidized bed using advanced measurement techniques. *Can J Chem Eng.* 2022;100:S272–S287. <https://doi.org/10.1002/cjce.24070>